

Electrochemical Corrosion Behavior of Atmospheric Plasma Sprayed Alumina Coatings

D.Thirumalaikumarasamy¹, K.Shanmugam², V. Balasubramanian³, R.Paventhan⁴

Assistant Professor, Department of Manufacturing Engineering, Annamalai University, Annamalainagar, Tamilnadu,
India¹

Associate Professor, Department of Manufacturing Engineering, Annamalai University, Annamalainagar, Tamilnadu,
India²

Professor, Department of Manufacturing Engineering, Annamalai University, Annamalainagar, Tamilnadu, India³

Professor, Department of Mechanical Engineering, Dhaanish Ahmed College of Engineering, Chennai, Tamilnadu,
India⁴

ABSTRACT: Alumina-based coatings are employed in many industrial applications, in order to protect the surface of metal components against high temperature, wear, corrosion and erosion. The corrosion deterioration process of plasma sprayed alumina coatings on AZ31B magnesium alloy was investigated using potentiodynamic polarization test in NaCl solution at different chloride ion concentrations, pH value and exposure time. Furthermore, an attempt was made to develop an empirical relationship to predict the effect of pH value, chloride ion concentration and exposure time on corrosion rate of plasma sprayed alumina coatings. The corroded surface was characterized by scanning electron microscopy (SEM) and X-ray diffraction (XRD). The results showed that the corrosion deterioration of alumina coated magnesium alloy in NaCl solutions was significantly influenced by chloride ion concentration and pH value. The alumina coatings were found to be highly susceptible to localized damage, and could not provide an effective corrosion protection to Mg alloy substrate in solutions containing acidic environments (pH3), higher chloride concentrations and exposure time.

KEYWORDS: Corrosion, Plasma spraying, Alumina coating, Mg alloy.

I. INTRODUCTION

Magnesium and its alloys, in the current era of persistently growing engineering demands, have become the most promising materials finding widespread applications in various industry segments such as automotive (various parts like steering columns, engine and transmission cases/covers, and seat frames), aerospace (gearbox housing and fuel pumps), portable electronic and communication devices (telephones, computers, and mobile phones), sporting goods, structural materials, handheld tools, household equipment, and biodegradable implants (orthopedic and trauma surgery). Besides being the 8th most abundant element on the earth, Magnesium (Mg) finds such a vast spectrum of applications based on the attractive engineering properties such as low density (1.74 g cm⁻³) coupled with high specific strength, excellent castability, workability, machinability and weldability, high thermal conductivity, good electromagnetic shielding characteristics, high vibration damping capacity, and a great recycling potential (Ferrando 1989; Song and Atrons, 1999).

Unfortunately, magnesium has a number of undesirable properties such as poor corrosion resistance resulting from inherently high chemical reactivity and significantly lower wear, and heat and creep resistance (Gray-Munro et al, 2008). Particularly, for the outdoor applications of magnesium, its susceptibility to galvanic corrosion eventually leads to severe pitting, resulting in the degradation of bulk and surface properties, which is a

International Journal of Innovative Research in Science, Engineering and Technology

(An ISO 3297: 2007 Certified Organization)

Vol. 3, Issue 12, December 2014

liability. This article discusses various means to reduce corrosion of Mg alloys, with a particular emphasis on atmospheric plasma spray (APS) coating as one of the available techniques (Singh et al, 2007).

The simplest route to protect Mg and its alloys has been to provide a coating on the top of metal substrate. Toward this, a host of engineering options such as anodizing, ion implantation, laser surface treatment (including surface melting, surface alloying composite surfacing, surface cladding, and shock peening), chemical conversion, electroplating, electroless plating, chemical vapor deposition (CVD), physical vapor deposition (PVD), diffusion coatings, organic/polymer coatings, and sol-gel coatings are available to protect the surface of Mg and its alloy components from its functional environment. The aforementioned processes were reviewed extensively by Gray and Luan, (2002) Blawert et al., (2006) and Singh and Harimkar (2012). While appreciating the potential advantages of each process, serious limitations exist with regard to the eco-friendliness, line-of-sight nature of the coating formation processes, toxic nature of the process bi-products, or the limited mechanical properties of the resultant coating such as low hardness, poor adhesion, and resistance to wear. Recently, the APS process has gained popularity as a coating technique that can protect Mg alloys.

Ceramic coatings are commonly employed for thermal and environmental protection of metal components operating at severe working conditions (Aruna et al.2012). Their application is able to improve the resistance and the durability of the underlying components, thus reducing the replacement of worn out parts and the related idle times. Among them Al_2O_3 coatings are good candidates for anti-wear and anti-corrosion applications, due to their high hardness, chemical inertness and high melting point, as well as to their high resistance to abrasion and erosion. Alumina coatings can retain up to 90% of their strength at 1100°C (Wang et al., 2000; Sarikaya, 2005). Despite of the fact that the coating materials themselves are highly corrosion resistant, existing defects in plasma sprayed ceramic coatings are detrimental to the corrosion resistance of such coated systems (Zhe Liu et al., 2013). Through-coating defects (e.g. pores) are particularly deleterious as they provide direct paths for corrosive electrolytes to reach the coating/substrate interface (Sugehis Liscano et al., 2004; Arrabal et al., 2009). Therefore, the internal microstructures of coatings play a big role in preventing or reducing corrosion attacks.

Various corrosion tests have been done to study the corrosion performance of the thermally sprayed coatings on magnesium alloys. In a buffer chloride solution, the corrosion rate of magnesium and its alloys did not depend on their purity or the content of the major alloying, but solely on the pH of the solution (Inoue et al., 2002). GUO Hui-xia et al. (2012) reported that MAO coating on AZ91D magnesium alloy had a better corrosion protection in dilute NaCl solution than in higher concentration NaCl solution. Martin et al. (2010) found that the general corrosion rate was higher for the immersion surfaces as compared to the salt spray surfaces, based on both thickness loss and weight loss. A study by Zhao et al. (2008) opined that the $Mg(OH)_2$ surface film on Mg alloys is probably formed by a precipitation reaction when the Mg^{2+} ion concentration at the corroding surface exceeds the solubility limit. Nandini Dinodi et al. (2013) reported that the environmental factors like temperature, concentrations of sulphate and chloride have a remarkable influence on rate of corrosion of magnesium alloy ZE41. Hara et al. (2007) studied the surface films formed by an open-circuit exposure to neutral solutions on the corrosion and their influence on the electrochemical behaviour of pure Mg and Mg alloys. The surface films were mainly composed of $Mg(OH)_2$ and grew rapidly during open-circuit exposure to 0.1 M NaCl solution and 0.1 M Na_2SO_4 solution. This indicated that the Mg was passivated in these two types of solutions.

From the literature review, (Inoue et al. 2002, GUO Hui-xia et al. 2012, Martin et al. 2010, Zhao et al. 2008, Nandini Dinodi et al. 2013 and Hara et al. 2007) it is understood that most of the published works have focused on the influence of pH and chloride ion concentrations on the corrosion of pure magnesium and magnesium alloys. From a practical view point, it is worthwhile to investigate and understand the effect of environmental factors on the corrosion behaviour of surface treated magnesium alloys. To date, however, there is not much published information on the effect of pH, chloride ion concentration and exposure time on the corrosion of surface treated magnesium alloys. Hence, by keeping the above points in mind, an investigation was carried out to develop an empirical relationship to predict the corrosion rate of plasma sprayed alumina coatings on AZ31B magnesium alloy under potentiodynamic polarization test. The effect of pH value, chloride ion concentration and exposure time on the corrosion behavior of plasma sprayed alumina coatings on AZ31B magnesium alloy is reported in this paper.

International Journal of Innovative Research in Science, Engineering and Technology

(An ISO 3297: 2007 Certified Organization)

Vol. 3, Issue 12, December 2014

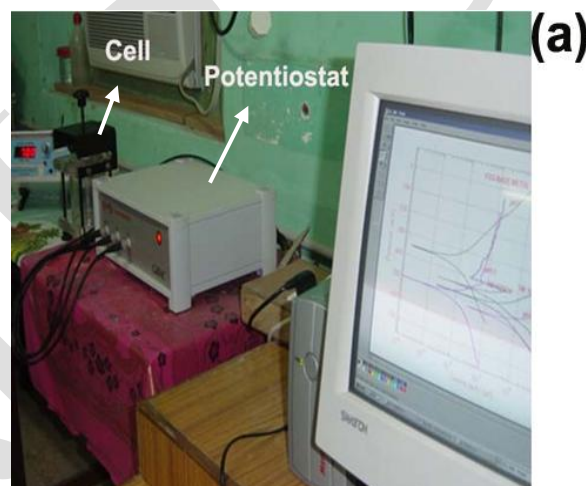
II. MATERIALS AND METHODS

The extruded rods of 15 mm thick AZ31B grade magnesium alloy were used in this investigation. The nominal chemical composition (wt.%) of experimental alloy AZ31B Mg was; Al—3.0%, Mn—0.2%, Zn—1.0%, and Mg—balance and it has the following mechanical properties: yield strength—171 MPa, ultimate tensile strength—215 MPa, elongation—14.7%, reduction in cross-sectional area—14.3%, and hardness at 0.05-kg load—69 Hv.

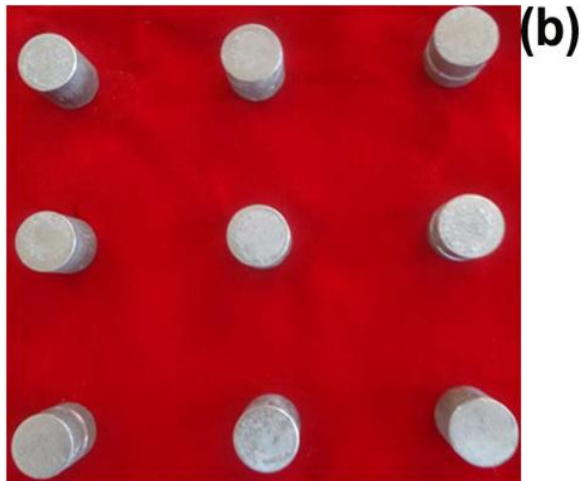
III. EXPERIMENTAL

In the present study, commercially available Al_2O_3 ceramic powder (AMPERIT 740.1) was identified as the coating material. The substrate coupons were of AZ31B magnesium alloy rod (BM). Substrates with the dimension of 16 mm \times 15 mm were grit-blasted on one side to clean and roughen the surface prior to deposition of the coating. Corundum, grit size of $320 \pm 500\mu\text{m}$ (Supplied by Metallizing Equipment Co. Jodhpur, India) was used to increase the surface roughness of the substrate. A surface roughness tester (Make: Mitutoyo, Japan; Model: Surf test 301) was used to measure the roughness and the average roughness of the substrate after grit blasting was found to be in the range of 5–10 μm . The optimized plasma spraying parameters, presented in Table 1, were used to deposit the coatings. The detailed characterisation, optimisation of APS process parameters and other relevant test procedures are explained in our previously published paper (Thirumalaikumarasamy et al., 2012). Commercial APS (Make: Ion Arc Technologies; India. Model: APSS-II) spraying system available at the Annamalai University, India, was used to deposit alumina coatings with a thickness of 240 μm . The thickness of the coatings was measured by a digital micrometer (with an accuracy of 0.001 mm) for each and every run conditions.

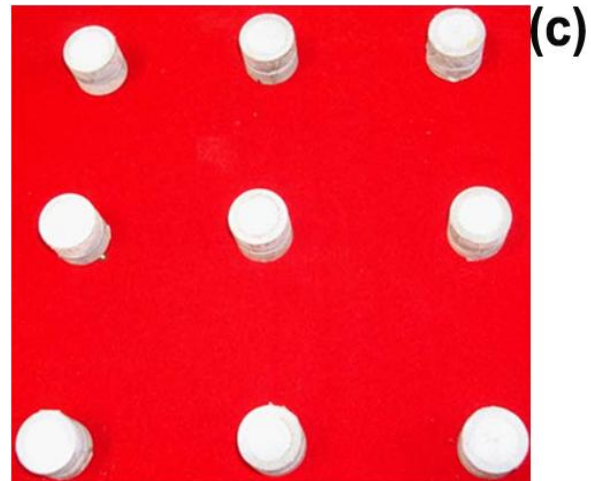
Potentiodynamic polarization test was carried out to evaluate the corrosion behavior of the alumina coated Mg alloys. The corrosion stability of coated samples was examined using a potentiodynamic test in NaCl solution at different chloride ion concentrations, pH value and exposure time. Photographs of plasma treated specimens were displayed in Figs. 1b and c.



Photograph of test set up



Photograph of uncoated specimens (after corrosion test)



Photograph of coated specimens (after corrosion test)

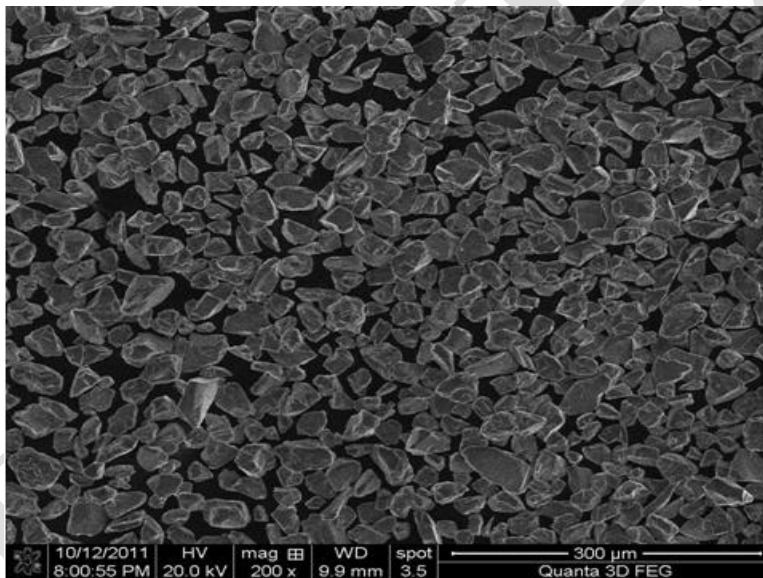


Fig.2 Scanning electron microscope (SEM) morphology of the as-purchased Al_2O_3 powders

Fig. 1 Details of potentiodynamic polarization test.

2.1 Structure and Composition

The Scanning Electron Microscope (Make: Jeol, Japan; Model: 6410-LV) was used to analyze the size and morphology of the parent materials. Fig. 2 shows the morphology of the as received powder under scanning electron microscope (SEM) with particle sizes in the range of -45 to $+20\mu m$. It can be seen in Fig. 2 that most of the powders present angular shape. Figure 3 shows the surface and cross-section morphology of alumina coating on AZ31B magnesium alloy. Compared with Fig. 2, it can be found in Fig. 3(a) that the sprayed alumina particles generate plastic deformation and hang together, which could be caused by the high velocity impact during plasma spraying. Meanwhile, in Fig. 3(b), it can be seen that the coating is very dense and the thickness is about $240\mu m$. There are no cracks and other defects found on the interface. And the AZ31B magnesium interface becomes irregular, which is from the grit-blasting surface preparation before the APS. Then, the accelerated alumina particles impact and embed onto the AZ31B substrate, leading to the plastic deformation on the AZ31B interface and thus inducing excellent bonding.

International Journal of Innovative Research in Science, Engineering and Technology

(An ISO 3297: 2007 Certified Organization)

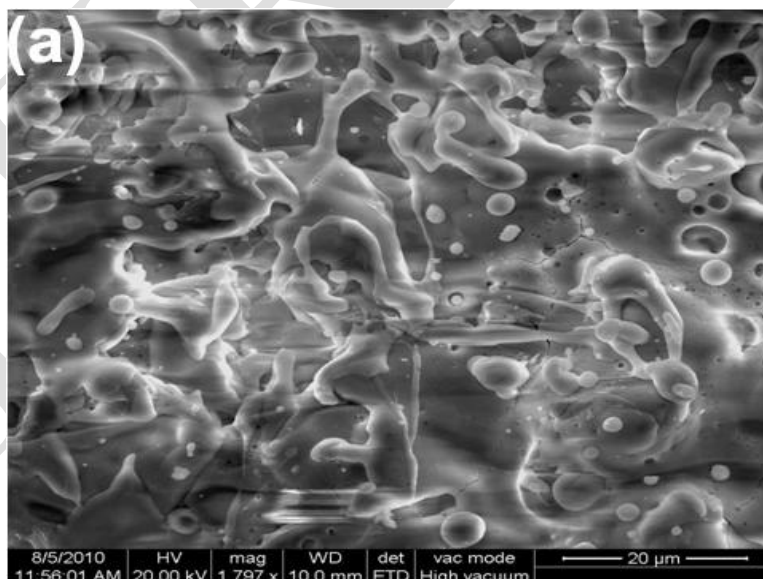
Vol. 3, Issue 12, December 2014

The main phases in the coating were detected using X-ray diffraction (XRD) experiment, in which the angle of the incident beam was fixed at 2° against the sample surface. The XRD profiles were recorded using Cu $K\alpha$ radiation at 40 kV and 20 mA. The XRD spectrum of the alumina coating is shown in Fig. 4. The coating was mainly constituted of both α - Al_2O_3 (JCPDS card no. 46-1212) and β - Al_2O_3 (JCPDS card no. 10-0425). The surface micrographs were observed by an optical microscope (Make: MEIJI, Japan; Model: MIL-7100).

2.2 Finding the limits of corrosion test parameters

From the published literature, (Inoue et al., 2002, GUO Hui-xia et al. 2012, Martin et al. 2010, Zhao et al . 2008, Nandini Dinodi et al. 2013 and Hara et al. 2007) and our laboratory investigations (Thirumalaikumarasamy et al., 2014) the predominant factors having significant influence on the corrosion behavior of AZ31B magnesium alloy are identified. They are: (i) pH value of the solution, (ii) chloride ion concentration and (iii) exposure time. Large numbers of trial experiments were conducted to identify the feasible testing conditions using plasma sprayed alumina coatings on AZ31B magnesium alloy under potentiodynamic polarization conditions. The following inferences were obtained:

- I. If the pH value of the solution was less than 3, the change in chloride ion concentration did not considerably affect the corrosion.
- II. If the pH value was in between 3 to 12, there was inhibition of the corrosion process and stabilization of the protective layer
- III. If the pH value was greater than 12, then blocking of further corrosion by the active centres of protective layer.
- IV. If the chloride ion concentration was less than 0.2M, then the visible corrosion did not occur in the experimental period.
- V. If the chloride ion concentration was in between 0.2M and 1M, then there was a reasonable variation in the corrosion rate.
- VI. If the chloride ion concentration was greater than 1M, then the rise in corrosion rate may hesitate and decrease a little.
- VII. If the exposure time was less than an 1hour, then the surface was fully covered with thick and rough corrosion products.
- VIII. If the exposure time was between 1 to 8 hours, then the tracks of the corrosion can be predicted.
- IX. If the exposure time was greater than 8 hours, then the tracks of corrosion film were difficult to identify.



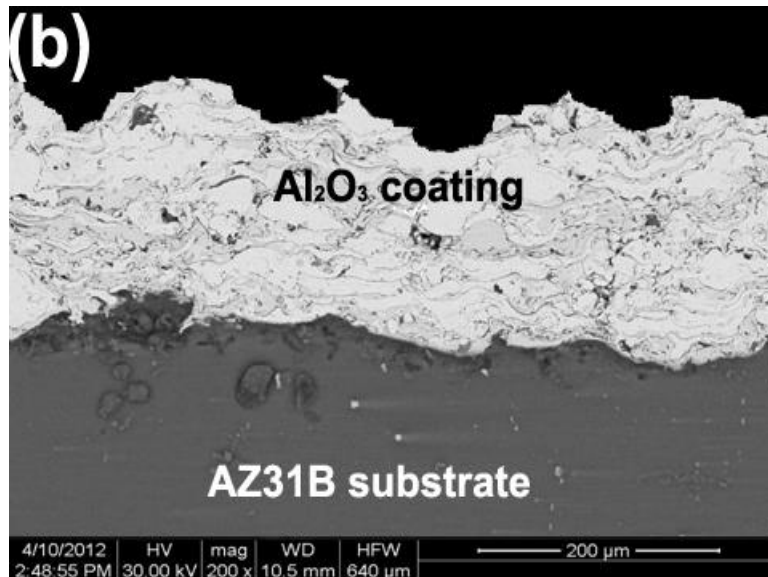


Fig.3 SEM morphologies of the Al₂O₃ coating (a) surface, (b) cross-section

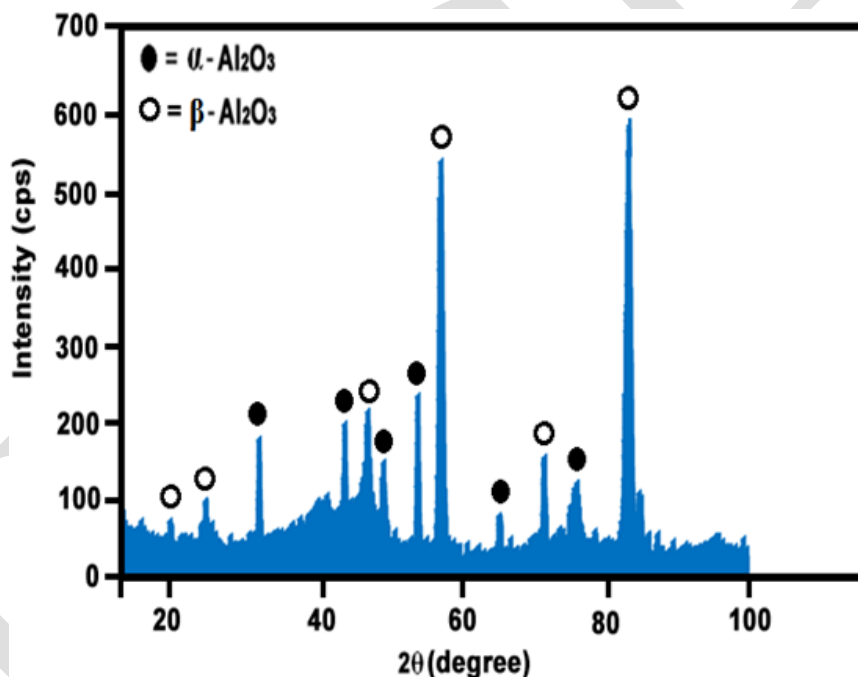


Fig. 4 XRD pattern of the alumina coating

2.3 Developing the design matrix

After considering all of the aforementioned conditions, the feasible limits of the parameters were chosen in such a way that the AZ31B magnesium alloy should be coated without any difficulty. A central composite rotatable design of second order was found to be the most efficient tool in response surface methodology (RSM) to establish the empirical relationship of the response surfaces using the smallest possible number of experiments without a loss of accuracy (Khuri and Cornell, 1996). Due to a wide range of factors, the use of a three-factors and five-level central composite design matrix was chosen to conduct the corrosion tests for the coatings. With a view to study the effects of

International Journal of Innovative Research in Science, Engineering and Technology

(An ISO 3297: 2007 Certified Organization)

Vol. 3, Issue 12, December 2014

the considered process parameters on the corrosion rate, statistically designed experiments, based on a factorial technique, were used to reduce the cost and time and to obtain the required information pertaining to the main and the interaction effects of the parameters on the response. The factors and their ranges considered for the corrosion test pertaining to the coatings are shown in Table 2. Tables 3 show the coded conditions of the corrosion test factors and their levels, which were used to form the design matrices for the coatings. The method of designing such a matrix is dealt with elsewhere (Miller et al., 1999). For the convenience of recording and processing experimental data, the upper and lower levels of the factors have been coded as +1.682 and -1.682, respectively. The coded values of the intermediate values can be calculated using the following relationship:

$$X_i = 1.682 [2X - (X_{max} + X_{min})] / (X_{max} - X_{min}) \dots\dots\dots (1)$$

Where,

X_i is the required coded value of a variable X and X is any value of the variable from X_{min} to X_{max} ;

X_{min} is the lower level of the variable;

X_{max} is the upper level of the variable.

2.4 Recording the Responses

The corrosion resistance of the coatings was determined by potentiodynamic test using an potentiostat/galvanostat (Make: ACM, UK; Model: Gill AC) with a corrosion software in NaCl solution at different chloride ion concentrations, pH value and exposure time. The potentiodynamic test was conducted in a 300 mL submarine-type three-electrode cell with the coated samples as a working electrode, a saturated calomel electrode (SCE) as a reference electrode, and platinum as a counter electrode. A one side of alumina coating was ground and contacted

Table I Optimized plasma spray parameters used to coat alumina

| Parameters | Unit | Values |
|-----------------------|------|--------|
| Power | kW | 22.27 |
| Primary gas flow rate | lpm | 35 |
| Stand-off distance | cm | 11.30 |
| Powder feed rate | gpm | 21.50 |
| Carrier gas flow rate | lpm | 7 |

Table II Important factors and their levels

| S.No | Factor | Notation | Unit | Levels | | | | |
|------|----------------------------|----------|-----------|--------|------|-----|-------|--------|
| | | | | -1.682 | -1 | 0 | +1 | +1.682 |
| 1 | pH value | <i>P</i> | - | 3 | 4.82 | 7.5 | 10.18 | 12 |
| 2 | Chloride ion concentration | <i>C</i> | Mole (M) | 0.2 | 0.36 | 0.6 | 0.84 | 1 |
| 3 | Exposure time | <i>T</i> | hours (h) | 1 | 2.42 | 4.5 | 6.58 | 8 |

with a conducting plate for electrical connection and the other side (1 cm²) was exposed to the electrolyte. After 10 min of initial delay, the potentiodynamic polarization curves were measured from -600 mV to 600 mV vs. open circuit potential (OCP) at a scan rate of 300 mV/min. Fig. 1 presents the details of corrosion test. All electrochemical tests were conducted in triplicate in order to ensure the reproducibility of results. The corrosion potential was developed and observed from the open circuit potential. Furthermore, corrosion current densities for all tests were measured directly from the tangent slope and it was recorded. Finally, the corrosion current densities (I_{corr}) for all tests were converted into the corrosion rate, using the molar mass and charge number.

International Journal of Innovative Research in Science, Engineering and Technology

(An ISO 3297: 2007 Certified Organization)

Vol. 3, Issue 12, December 2014

The corrosion rate can be calculated using Faraday’s Law, in terms of penetration rates as per ASTM G 102 (2004). This standard practice is intended to provide guidance in converting the results of electrochemical measurements to rates of uniform corrosion. The calculation methods for converting the corrosion current density values to either mass loss rates or average penetration rates, are given for most engineering alloys. The corrosion rate can be calculated from the current density using Faraday’s law, given by Eqn. 2

$$\text{Corrosion rate (mm/ year)} = m \times I_{\text{corr}} / z \times \rho \times f \dots\dots\dots(2)$$

In Eqn.2, the Faraday constant F is 96485.34 C mol⁻¹, the atomic mass m is 26.82 g mol⁻¹, the electron number z is 2, ρ is the density of the coated samples, the corrosion rate is in mm/yr and the current density (I_{corr}) is in Am⁻².

Table III Design matrix ad Experimental results

| Experiment Number | Coded values | | | Original values | | | Corrosion rate (mm/year) |
|-------------------|--------------|-------|-------|-----------------|-------|----------|--------------------------|
| | P | C | T | P (pH) | C (M) | T (hour) | |
| 1 | -1.00 | -1.00 | -1.00 | 4.82 | 0.36 | 2.42 | 2.72 |
| 2 | 1.00 | -1.00 | -1.00 | 10.18 | 0.36 | 2.42 | 1.46 |
| 3 | -1.00 | 1.00 | -1.00 | 4.82 | 0.84 | 2.42 | 2.28 |
| 4 | 1.00 | 1.00 | -1.00 | 10.18 | 0.84 | 2.42 | 1.10 |
| 5 | -1.00 | -1.00 | 1.00 | 4.82 | 0.36 | 6.58 | 4.02 |
| 6 | 1.00 | -1.00 | 1.00 | 10.18 | 0.36 | 6.58 | 3.88 |
| 7 | -1.00 | 1.00 | 1.00 | 4.82 | 0.84 | 6.58 | 4.36 |
| 8 | 1.00 | 1.00 | 1.00 | 10.18 | 0.84 | 6.58 | 3.47 |
| 9 | -1.68 | 0.00 | 0.00 | 3 | 0.6 | 4.5 | 5.69 |
| 10 | 1.68 | 0.00 | 0.00 | 12 | 0.6 | 4.5 | 2.57 |
| 11 | 0.00 | -1.68 | 0.00 | 7.5 | 0.2 | 4.5 | 1.51 |
| 12 | 0.00 | 1.68 | 0.00 | 7.5 | 1 | 4.5 | 3.92 |
| 13 | 0.00 | 0.00 | -1.68 | 7.5 | 0.6 | 1 | 3.24 |
| 14 | 0.00 | 0.00 | 1.68 | 7.5 | 0.6 | 8 | 2.05 |
| 15 | 0.00 | 0.00 | 0.00 | 7.5 | 0.6 | 4.5 | 3.15 |
| 16 | 0.00 | 0.00 | 0.00 | 7.5 | 0.6 | 4.5 | 2.85 |
| 17 | 0.00 | 0.00 | 0.00 | 7.5 | 0.6 | 4.5 | 3.13 |
| 18 | 0.00 | 0.00 | 0.00 | 7.5 | 0.6 | 4.5 | 2.94 |

International Journal of Innovative Research in Science, Engineering and Technology

(An ISO 3297: 2007 Certified Organization)

Vol. 3, Issue 12, December 2014

| | | | | | | | |
|----|------|------|------|-----|-----|-----|------|
| 19 | 0.00 | 0.00 | 0.00 | 7.5 | 0.6 | 4.5 | 3.08 |
| 20 | 0.00 | 0.00 | 0.00 | 7.5 | 0.6 | 4.5 | 2.90 |

IV. PREDICTIVE STATISTICAL MODEL FOR CORROSION RATE

In this study, a response surface model-building technique was utilised to predict the corrosion rate in terms of the pH value, chloride ion concentration and exposure time. Details of the model-building technique are discussed below.

3.1. Response surface methodology (RSM)

RSM is an experimental strategy that explores the space of the process independent variables and an empirical statistical modeling, to develop an appropriate relationship between the responses (output) and the process variables or factors (input) (Kumar et al., 2007). In the present investigation, to correlate the process parameters and the

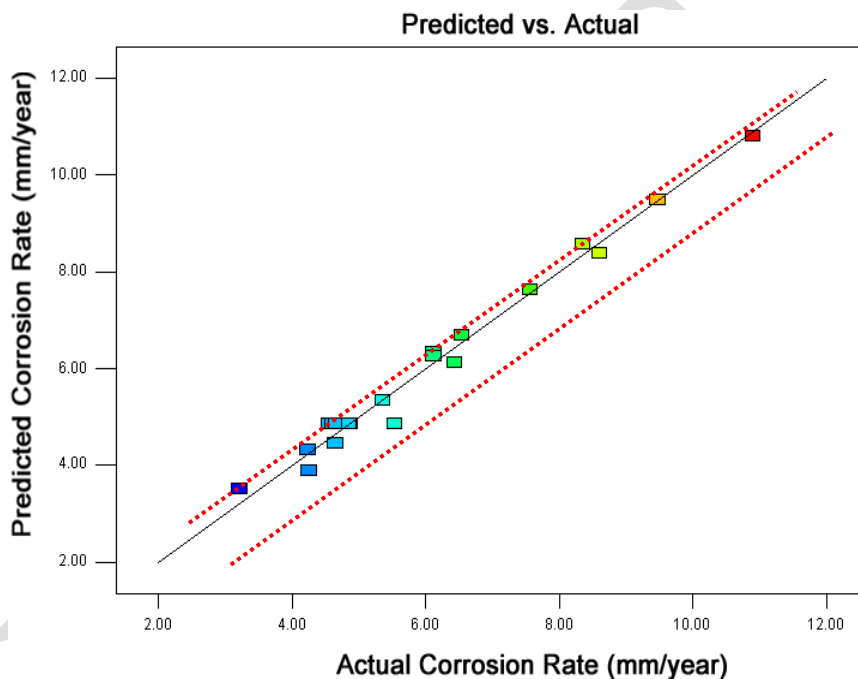


Fig.5 Correlation plot for the response

corrosion rates, a second order quadratic empirical relationship was developed to predict the responses based on experimentally measured values. The responses are a function of pH value (P), chloride ion concentration (C), exposure time (T) and it can be expressed as

$$\text{Corrosion rate (CR)} = f(P, C, T) \dots \dots \dots (3)$$

The empirical relationship chosen includes the effects of the main and interaction effect of all factors. The construction of polynomial empirical relationship and the procedure to calculate the values of the regression coefficients can be referred elsewhere (Benyounis and Olabi, 2008). In this work, the regression coefficients were calculated with the help of Design Expert V 8.1 statistical software. After determining the coefficients (at a 95% confidence level), the final empirical relationships were developed using these coefficients. The final empirical relationship to estimate the corrosion rate of plasma sprayed alumina coatings on AZ31B magnesium alloy is given below,

$$\text{Corrosion rate (CR)} = \{0.56 + 0.085(P) + 0.014(C) - 0.052(T) + 0.035(PT) + 0.051(CT) + 0.042(C^2)\} \text{ mm/year} \dots \dots \dots (4)$$

International Journal of Innovative Research in Science, Engineering and Technology

(An ISO 3297: 2007 Certified Organization)

Vol. 3, Issue 12, December 2014

The adequacy of the developed models was tested using the analysis of variance (ANOVA) technique. As per this technique, if the calculated value of F_{ratio} of the developed model is less than the standard F_{ratio} (from F-table) value at a desired level of confidence (say 99%), then the model is said to be adequate within the confidence limit. ANOVA test results for the responses are presented in Table 4. From the table, it can be understood that the developed model is adequate to predict the corrosion rate of plasma sprayed alumina coatings on AZ31B magnesium alloy at 95%

Table 4 ANOVA test results

| Source | Sum of squares | df | Mean Square | F value | p-value Prob > F | |
|-----------------------|----------------|----|-------------|---------|---------------------|------------------------|
| Model | 0.46 | 9 | 0.051 | 38.62 | < 0.0001 | Significant |
| <i>P</i> | 0.095 | 1 | 0.095 | 74.98 | < 0.0001 | |
| <i>C</i> | 0.26 | 1 | 0.26 | 196.08 | < 0.0001 | |
| <i>T</i> | 0.034 | 1 | 0.034 | 28.34 | 0.0003 | |
| <i>PC</i> | 4.652E-003 | 1 | 4.652E-003 | 3.54 | 0.0880 | |
| <i>PT</i> | 9.886E-003 | 1 | 9.886E-003 | 7.53 | 0.0206 | |
| <i>CT</i> | 0.022 | 1 | 0.022 | 15.61 | 0.0026 | |
| <i>P</i> ² | 1.545E-004 | 1 | 1.545E-004 | 0.12 | 0.7384 | |
| <i>C</i> ² | 0.025 | 1 | 0.025 | 19.57 | 0.0012 | |
| <i>T</i> ² | 1.103E-003 | 1 | 1.103E-003 | 0.83 | 0.3807 | |
| Residual | 0.013 | 10 | 1.311E-003 | | | |
| Lack of Fit | 9.712E-003 | 5 | 9.712E-003 | 2.84 | 0.1370 | Not significant |
| Pure Error | 3.400E-003 | 5 | 6.800E-004 | | | |
| Cor Total | 0.47 | 19 | | | | |

confidence level. Value of “prob > F” less than 0.0500 indicated model terms are significant. In this corrosion test P, C, T, PT, TC and T² are significant model terms for plasma sprayed alumina coatings on AZ31B magnesium alloy. Further, each observed value matches its experimental value well, as shown in Fig. 5.

V. DISCUSSION

4.1 Effect of pH value on corrosion rate

Fig.6 represents the effect of pH on corrosion behavior of plasma sprayed alumina coating on AZ31B magnesium alloy in NaCl solution. From Fig.6 it could be inferred that, if the pH value increases, the corrosion rate decreases (Liang et al., 2010). At every chloride ion concentration and time, the coatings usually exhibited a decrease in corrosion rate with the increase in pH. The highest corrosion rate was observed at pH 3 and at neutral pH, the corrosion rate was remained constant approximately and comparatively low corrosion rate was observed in alkaline solution. It was seen that the influence of pH was more at higher concentration as compared to lower concentration in neutral and alkaline solutions (Gou yin-ning et al., 2010).

**International Journal of Innovative Research in Science,
Engineering and Technology**

(An ISO 3297: 2007 Certified Organization)

Vol. 3, Issue 12, December 2014

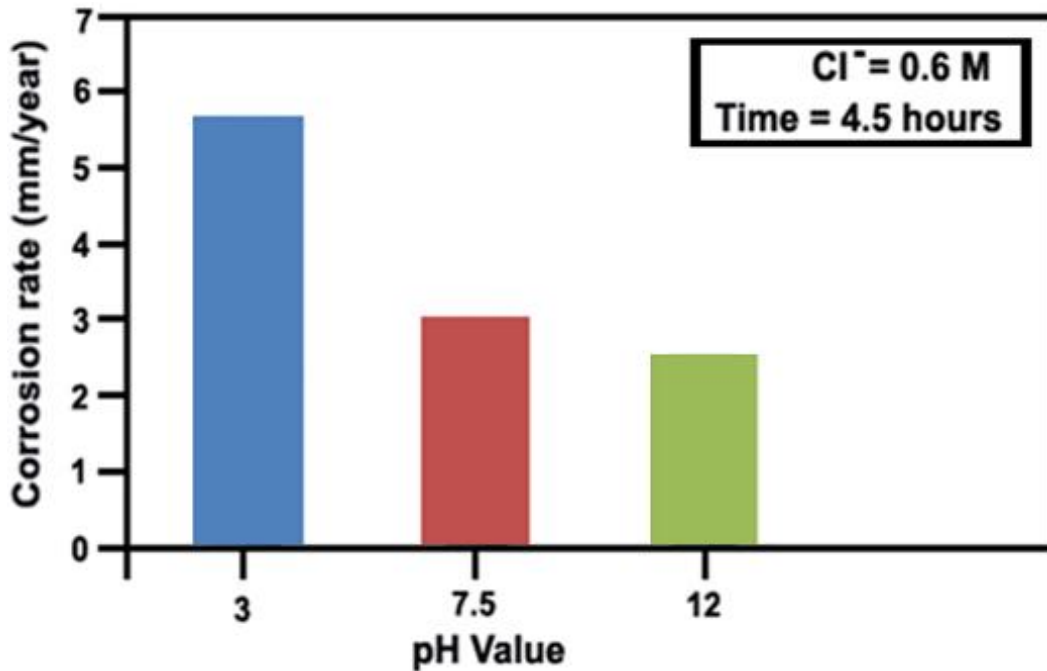


Fig.6 Effect of pH value on corrosion rate

At lower pH values, the alumina coating exhibited a rise in corrosion rate with an increase in chloride ion concentration. But the quantity of this rise was different in such a way that, the change in chloride ion concentration at lower concentrations affected the corrosion rate much more as compared to that of higher concentration. It showed that with the increase in chloride ion concentration, the rising rate at corrosion rate decreased that is, the influence of chloride ion concentration was much lower at higher concentrations.

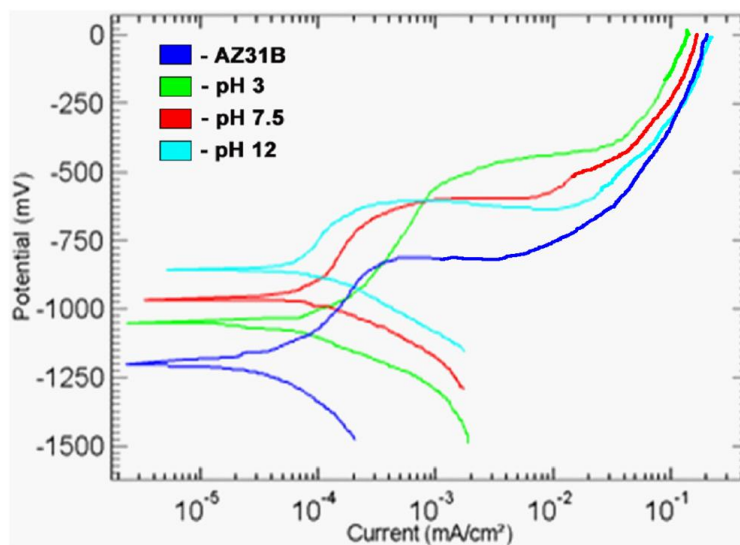


Fig.7 Effect of pH on tafel plots

Fig. 7 displays the effect of the pH value on the Tafel plots from the potentiodynamic polarization test at different pH values. It is observed that with the decreasing pH value of the solutions, the anodic curve of the materials showed a shift to more negative (more active) potential. It is found that the corrosion rate usually increased with the decrease in

International Journal of Innovative Research in Science, Engineering and Technology

(An ISO 3297: 2007 Certified Organization)

Vol. 3, Issue 12, December 2014

the pH values of the solutions (Yun TIAN et al., 2011). The anodic curve of the materials showed a shift to lower current density values, with the increase in the pH value. With the increment of the pH value the potential increases, which means the dissolution of magnesium in aqueous solutions proceeds by the reduction of water to produce magnesium hydroxide. The reduction process includes mainly water, which could be reduced, thus forming a $Mg(OH)_2$ protective layer. Higher pH values favor the formation of $Mg(OH)_2$ which reduces corrosion. Furthermore, the cathodic process is remarkably retarded with the increase in the pH value. This is evident from the wider plot of the cathodic curve, with decreasing pH values.

The effect of pH on the pit morphology of the base metal and coated specimens were shown in Fig. 8. It could be inferred from the figure that, at lower pH values, the pit becomes wider and deeper but at higher pH values; the pit seems to be narrow. This means, if a corroding area is adjacent to a non-corroded area, there will be a galvanic cell causing the galvanic acceleration of the corrosion rate of the non-corroded area in an acidic medium. Thus, once the corrosion starts, there is an electrochemical driving force for the spread of the corrosion across the surface. The accumulation of Mg ions in the pit induced the electric migration of the chloride ions into the pit. Hence, it causes the anodic dissolution of Mg inside the pit. This is indeed what is observed experimentally. In a neutral condition, it is observed that the pit area and pit depth decrease, which means, the galvanic acceleration of corrosion across the non-corroding areas is balanced by the galvanic protection of the corroded areas, so that the corrosion tends to be rather shallow in the corroded areas. Also, it is noted that, with the increase in the pH value, i.e., in alkaline media, the pit depth and pit area decrease. The presence of OH^- ions in alkaline media allows the formation of $Mg(OH)_2$, an insoluble layer, which decreases the corrosion attack within the pit.

The SEM micrograph and scanned images of the corroded specimens Fig.9 reveals the at lower pH values, the alumina coated specimen which suffered a severe chemical dissolution in exposed area, the alumina coating flaked-off in a few regions. The coating was not stable in this acidic electrolyte, and was found to have been damaged at localized regions (Fig.9a). Thus, the magnesium substrate underneath the coating was exposed to the electrolyte. The flake off of larger coating areas in acidic solutions was caused possibly by hydrogen gas evolution and the formation of corrosion products after the acidic solution reaches the interface between the coating and the magnesium alloy substrate, because the quick increase of pressure and/or volume in the limited space of the pores caused high stresses. It was also believed that the higher pore density of the coating and higher amount of second phase may have a strong influence on the tendency for flaking. As a consequence, the alumina coating, which had a higher pore density and higher amounts of second phase, was found to be vulnerable to this form of damage. It meant that the pH value was one of the major factors of corrosion rate.

In the NaCl solution of pH 7.5, there was no pronounced corrosion damage on the surface of the alumina coated specimen and at the same time, the corrosion resistance kept nearly the same throughout the test period as can be seen from Fig.9b. Furthermore, SEM micrograph (Fig.9b) revealed that the coating surface did not undergo any discernible corrosion degradation. It is thus evident in this case that the alumina film at the interface was very stable and could resist the corrosion damage. These results indicated that the alumina coating could survive much longer time in neutral NaCl solution without any signs of degradation. When the pH of NaCl solution was increased to 12, the alumina coated specimen exhibited a higher corrosion resistance and a more stable behavior than those in the acidic and neutral solutions (Fig.9c). It is clear from the Fig.9c, no obvious damage and coating degradation was observed on the surface of the material.

4.2 Effect of chloride ion concentration on corrosion rate

The influence of chloride ion concentration on corrosion rates of plasma sprayed alumina coating on AZ31B magnesium alloy are illustrated in the Fig.10. It is seen that the coatings exhibited a rise in corrosion rate with the increase in Cl^- concentration and thus the change of Cl^- concentration affected the corrosion rate much more in higher concentration solutions than that in lower concentration solutions. When more Cl^- in NaCl solution promoted the corrosion, the corrosive intermediate (Cl^-) would be rapidly transferred through the outer layer and reached the coated surface (Liang et al., 2010). Hence, the corrosion rate was increased.

**International Journal of Innovative Research in Science,
Engineering and Technology**

(An ISO 3297: 2007 Certified Organization)

Vol. 3, Issue 12, December 2014

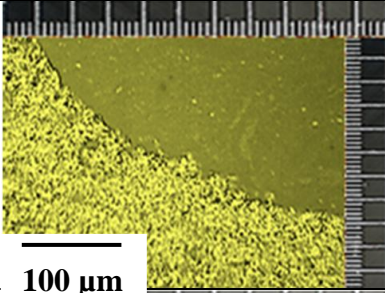
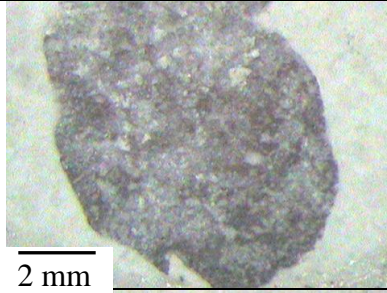
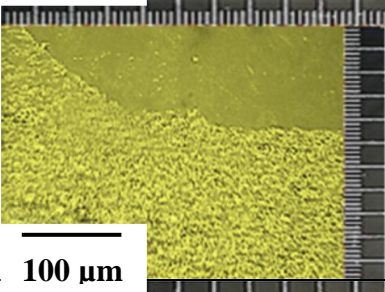
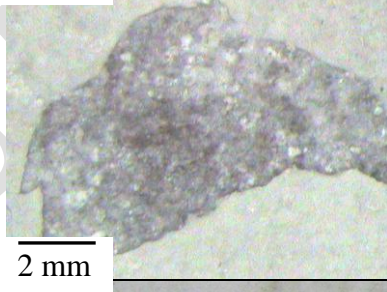
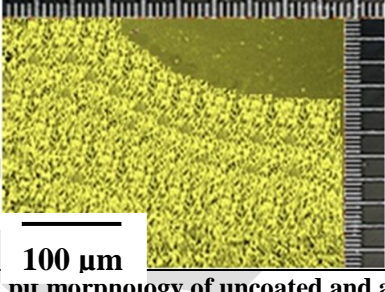
| | AZ31B magnesium alloy | Plasma sprayed Al ₂ O ₃ coatings |
|---|---|---|
| (a) pH=3, Time=4.5h, Cl ⁻ =0.6M |  |  |
| (b) pH=7.5, Time=4.5h, Cl ⁻ =0.6M |  |  |
| (c) pH=12, Time=4.5h, Cl ⁻ =0.6M |  |  |

Fig.8 Effect of pH value on pit morphology of uncoated and alumina coated AZ31B Mg alloy

Fig. 11 reveals the effect of the chloride ion concentration on the Tafel plots from the pitting corrosion test at different chloride ion concentration. It is observed that with the increase in chloride ion concentration of the solutions, the anodic curve of the materials showed a shift to higher current density values. The corrosion potential shifted to more negative (active) values with the increase in the chloride ion concentration. Furthermore, the cathodic process is remarkably retarded with the increase of the pH value. This was evident from the wider plot of the cathodic curve with the decreasing pH value (Yang Yue and Wu Hua, 2010). This is due to the adsorption of the chloride ion on the alloy surface at weak parts of the oxide film. Thus, the increase in the corrosion rate with the increasing chloride ion concentration contributed to the participation of the chloride ions in the dissolution reaction.

Fig. 12 clearly reveals that, the pit seems to be narrowed, at lower chloride ion concentration, but at higher concentration, the pit became wider and shallow. Also, the pit depth increased with the increase in the concentration of the solution for both the uncoated and as coated specimens. It is found that anodic dissolution was

**International Journal of Innovative Research in Science,
Engineering and Technology**

(An ISO 3297: 2007 Certified Organization)

Vol. 3, Issue 12, December 2014

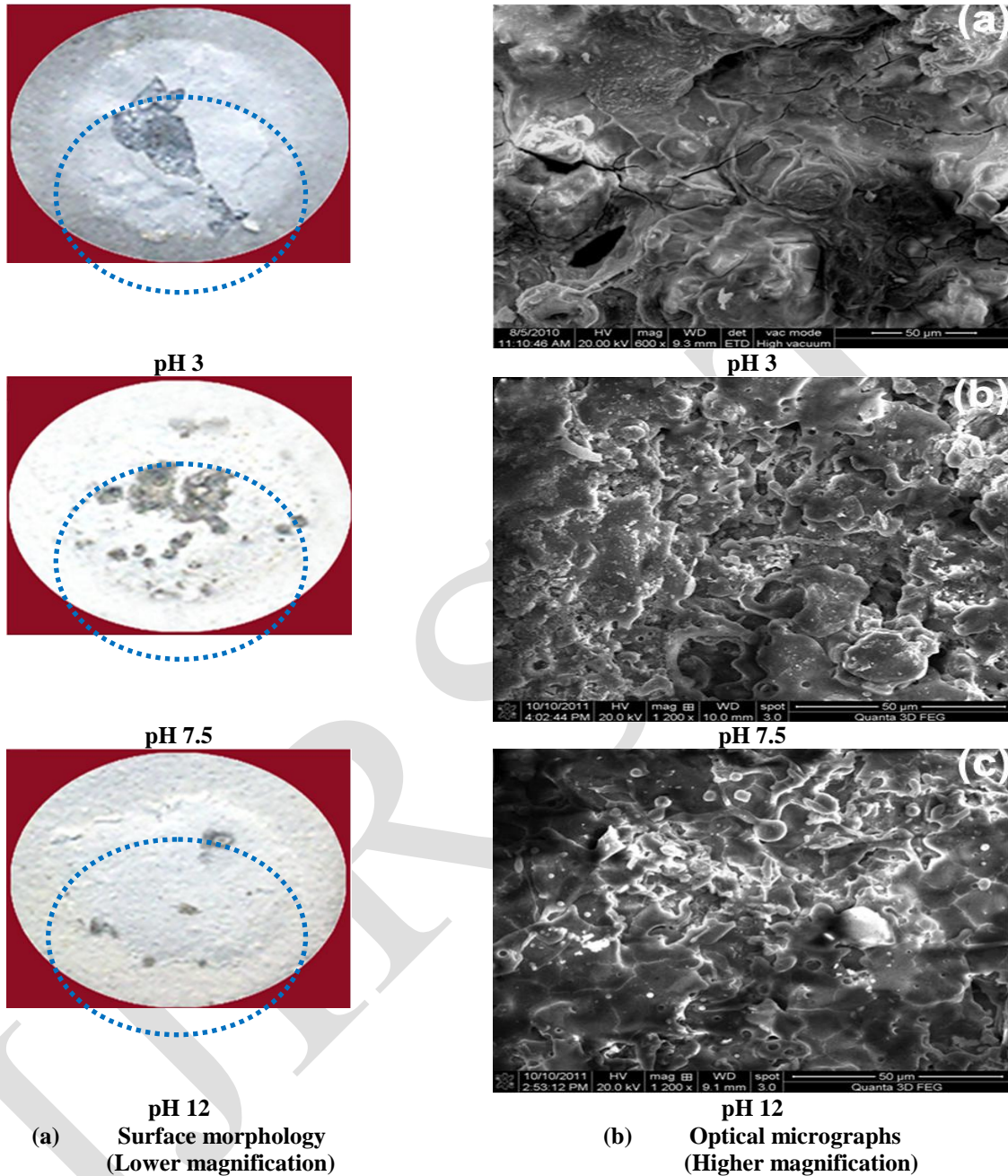


Fig.9 Effect of pH on corrosion morphology of alumina coatings on AZ31B magnesium alloy

**International Journal of Innovative Research in Science,
Engineering and Technology**

(An ISO 3297: 2007 Certified Organization)

Vol. 3, Issue 12, December 2014

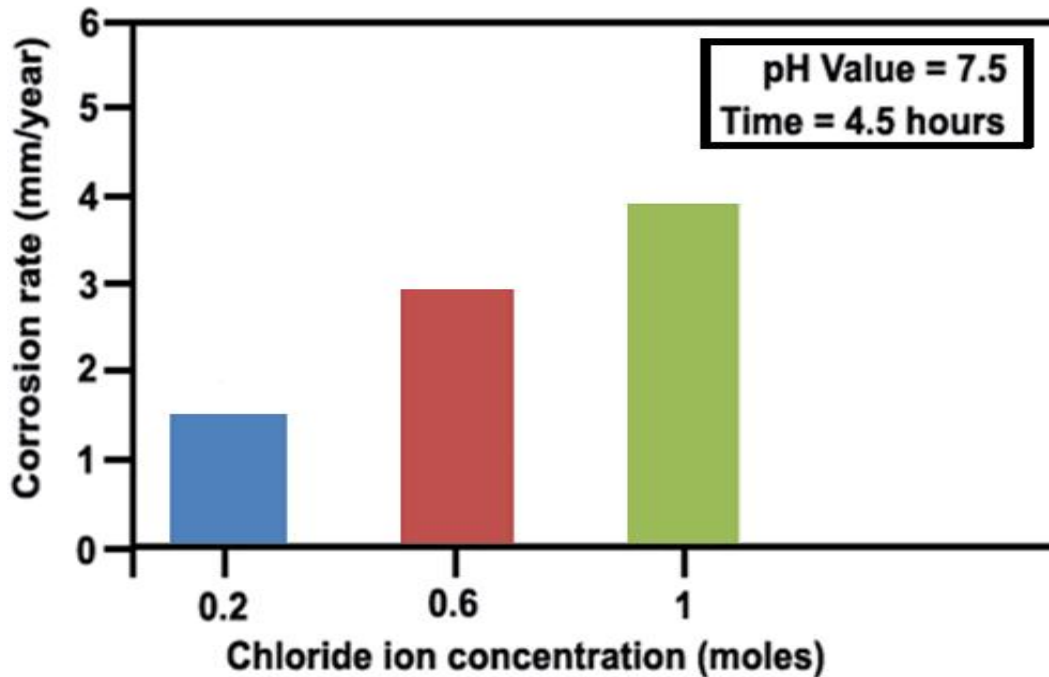


Fig.10 Effect of chloride ion concentration on corrosion rate

observed inside the pit. During anodic dissolution, the second phase particles dissolve with the dissolving Mg and form the corrosion pits. Then the ion is de-oxidized by the magnesium, and is deposited on the surface of the magnesium alloy as an oxide film. The successive oxidized film is destroyed by the sediment. Hence, chloride

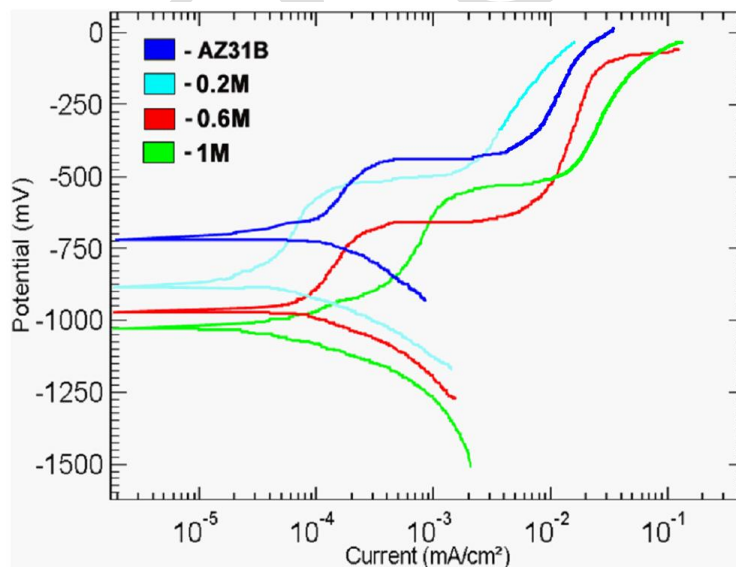


Fig.11 Effect of chloride ion concentration on tafel plot

accumulation within the pit accelerates anodic dissolution. It is also found that, inside the pit, the whole α -grains undergo a major part of corrosion, and the border of the corroded area is mostly surrounded by the β -phase. This might be attributed to the more negative potential of the α -phase than that of the β -phase in the NaCl solutions. There is a tendency for the corrosion rate by micro-galvanic coupling of the α -phase to be accelerated between the α -phase

International Journal of Innovative Research in Science, Engineering and Technology

(An ISO 3297: 2007 Certified Organization)

Vol. 3, Issue 12, December 2014

and the β -phase. The increasing trend of the pit depth and area with the increase in the chloride ion concentration is attributed to the attack of the Cl^- ions on the surface, leading to the anodic dissolution of Mg.

As shown in the SEM micrograph and scanned images Fig.13, it is also observed that at lower chloride ion concentrations, coating has no pronounced deterioration in this condition. At this stage, because the pores and defects were not interconnecting and chloride ion concentration in 0.2M NaCl solution was low, the corrosive electrolyte permeated slowly into the coating through these intrinsic defects. In lower chloride ion concentration solutions (0.2M NaCl), because the corrosive electrolytes are too mild to break down the coatings, the corrosion deterioration of coated specimens was dictated by the degradation of coatings especially in inner regions of the coating. Therefore, due to the denser and more compact inner layer in the alumina coating was superior and the corrosion deterioration was slower in mild corrosive electrolytes (Fig.13a).

In the more concentrated electrolytes (1M NaCl), however, the permeation of higher concentration of chloride ions into the coating/substrate interface induced the quick breakdown of alumina coatings and caused a localized damage on the underneath magnesium alloy substrate. The level of corrosion damage increased with the increase of chloride ion concentration of NaCl solution. At the concentration not more than 0.2M, the coating was only deteriorated lightly on the edge of the samples. However, when the ion concentration reaches 1M, a large amount of chloride ions penetrate the coating and contact with the substrate, resulting in heavy corrosion reaction and a larger level of corrosion damage (Fig.13c). Based on this investigation, it is concluded that the alumina coatings cannot provide a long term protection to the magnesium alloy substrate in neutral environments containing high chloride concentrations (Song et al., 2012).

4.3 Effect of exposure time on corrosion rate

Fig. 14 depicts the influence of the exposure time on the corrosion rate of alumina coatings on AZ31B magnesium alloy. From the figure, it can be inferred that the corrosion rate decreased with the increase in exposure time. It proves that the initial corrosion product impeded the passage of corrosion medium and provided protection for the coated specimen. In long time exposure with magnesium dissolution and hydrogen evolution, the pH value of the solution will increase, namely basification. Basification should be propitious to the formation of passive film, which can protect the alloy. The insoluble corrosion products on the surface of the alloy could slow down the corrosion rate.

The effect of exposure time on the tafel plots is shown in Figure 15. The corrosion potential shifted to a more positive direction with the increase in the exposure time, while the anodic curve of the materials shows a shift to lower current density values, indicating that anodic dissolution is retarded, with the increase in the exposure time (Fig. 15). As a result, the corrosion current also decreases with increasing exposure time (Suegama et al., 2005). Furthermore, the cathodic process is remarkably retarded with the increase of the exposure time. This was evident from the wider plot of the cathodic curve with decreasing exposure time.

Fig. 16 reveals the effect of exposure time on the pit morphology of the samples. For both the substrate and coatings examined, microscopic observations of the corroded surfaces indicated that the lower exposure time, the pit became deeper but with higher exposure time, the pit seems a little wider, possessing large corroded products. This means that with the increase in pit depth, the pit area decreases, and the increase in the pit area tends to decrease the pit depth (Fig. 16). This is due to the specimen being continuously exposed to the NaCl solution, when general corrosion could occur alongside pitting corrosion. The decrease in the pit depth with greater exposure time, is the result of general corrosion removing the area surrounding the pits, while the pit grows downwards. At an earlier stage, the water present in the NaCl solution allows the formation of a $\text{Mg}(\text{OH})_2$ film, that is immediately degraded by further corrosion. Subsequently there is no protective behavior by the film. The continuous

**International Journal of Innovative Research in Science,
Engineering and Technology**

(An ISO 3297: 2007 Certified Organization)

Vol. 3, Issue 12, December 2014

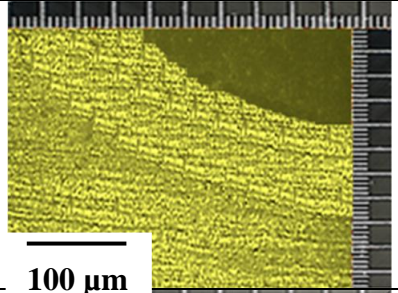
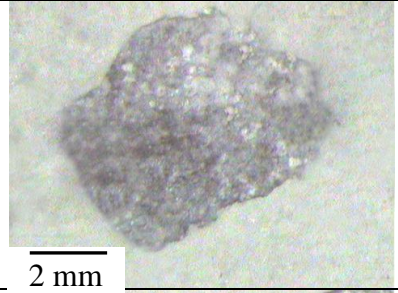
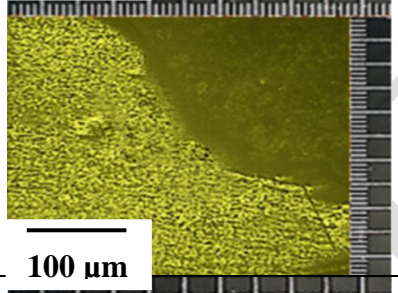
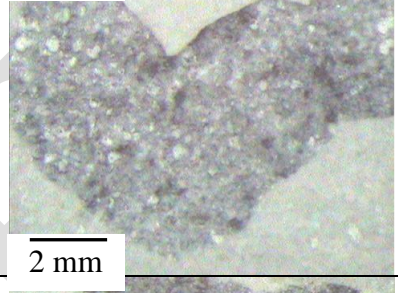
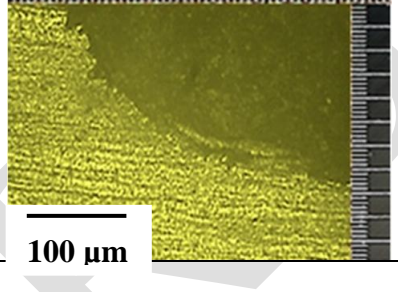
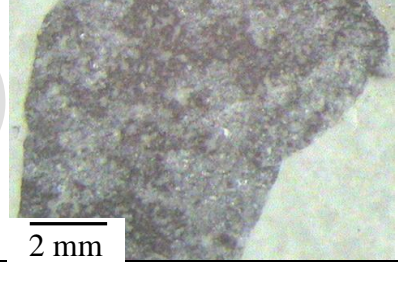
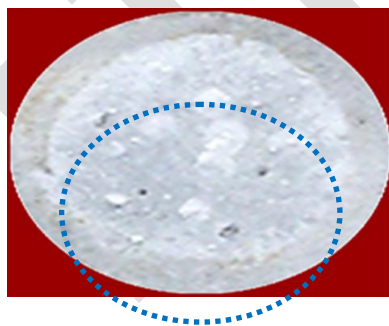
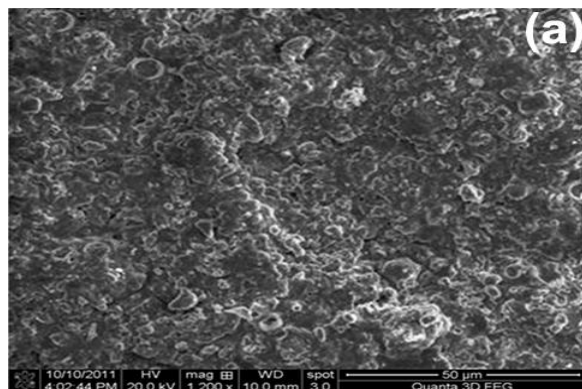
| | AZ31B magnesium alloy | Plasma sprayed Al ₂ O ₃ coatings |
|---|---|--|
| (a) pH=7.5, Time=4.5h, Cl ⁻ =0.2M |  |  |
| (b) pH=7.5, Time=4.5h, Cl ⁻ =0.6M |  |  |
| (c) pH=7.5, Time=4.5h, Cl ⁻ =1M |  |  |

Fig.12 Effect of chloride ion concentration on pit morphology of of uncoated and alumina coated AZ31B Mg alloy



Cl⁻ = 0.2 M



Cl⁻ = 0.2 M

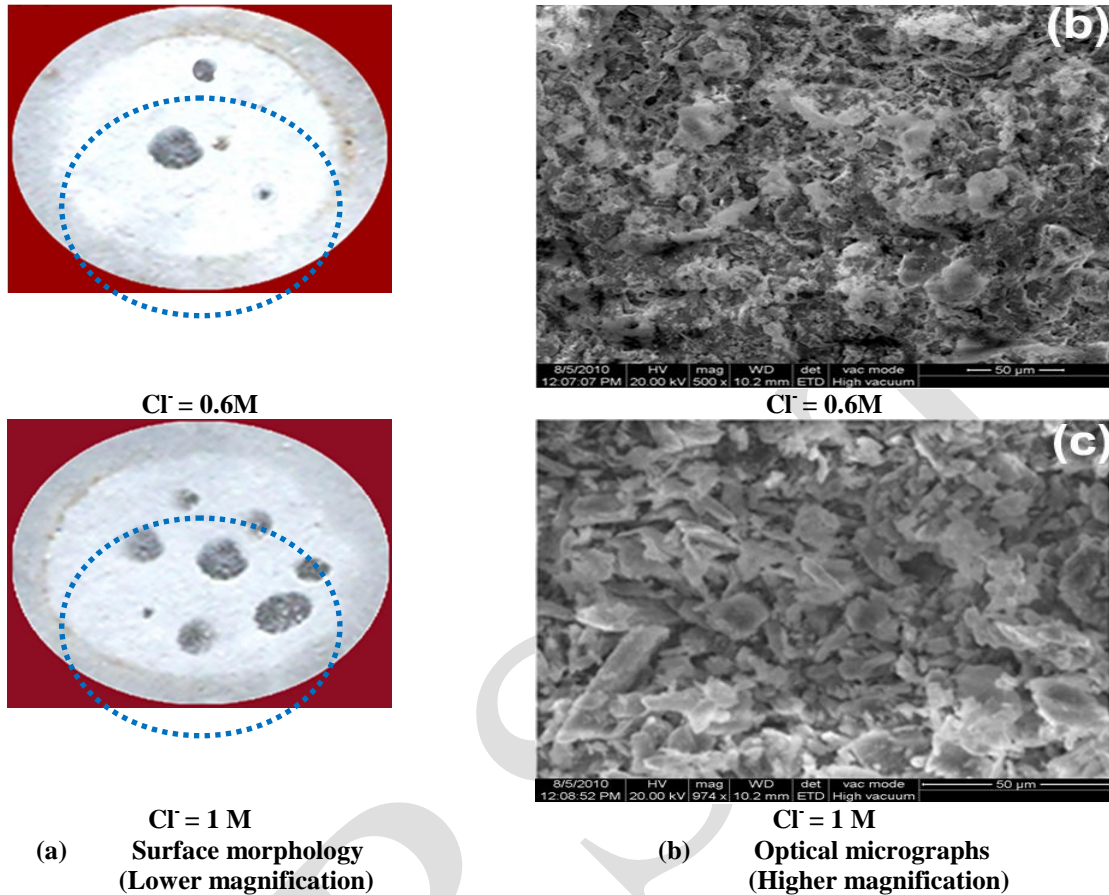


Fig.13 Effect of chloride ion concentration on corrosion morphology of alumina coatings on AZ31B magnesium alloy

formation and degradation of the film cause the pit to stop growing in depth. At 4.5h, when the general corrosion becomes fully dominant, the growth of the pit depth could no longer keep pace with general corrosion, meaning that the pit area gradually increases as the magnesium within the pits is removed along with the magnesium surrounding the pits.

The SEM micrograph of the coating after 1h of exposure is shown in Fig.17a, where no obvious indication of blistering of the coating can be observed. However, the coating seems to be locally attacked in some areas inside the coating (noted as arrows in Fig. 17a). As expected, the attacked areas are confined essentially at the base of the micro cracks as shown by white arrows in Fig. 17a. The microcracks are favourable sites for micro galvanic and/or micro crevice corrosion of thermal spray coatings as reported in the literature (You Wang et al., 2009). As discussed before, faster diffusion of small Cl⁻ ions than that of oxygen occurring in these regions can limit the passive behavior of the coatings. After 4.5 hour of exposure, the SEM micrograph in Fig. 17b showed that these damaged regions were swelled and had corrosion products on it. At the same time, relatively slight corrosion damage occurred in some other regions of this exposed area (Fig. 17b) and interestingly, the corrosion damage was confined mostly to the micro pores. The SEM micrograph of alumina coating after 8 hour of exposure showed that unlike the APS coating, localised attack can be detected (Fig. 17c) through the coating surface. In the case of APS coating, micro cracks and intersplat oxides are responsible for the electrolyte penetration into the coating. A localised corrosion can also take place at these defects which attacks the coating body.

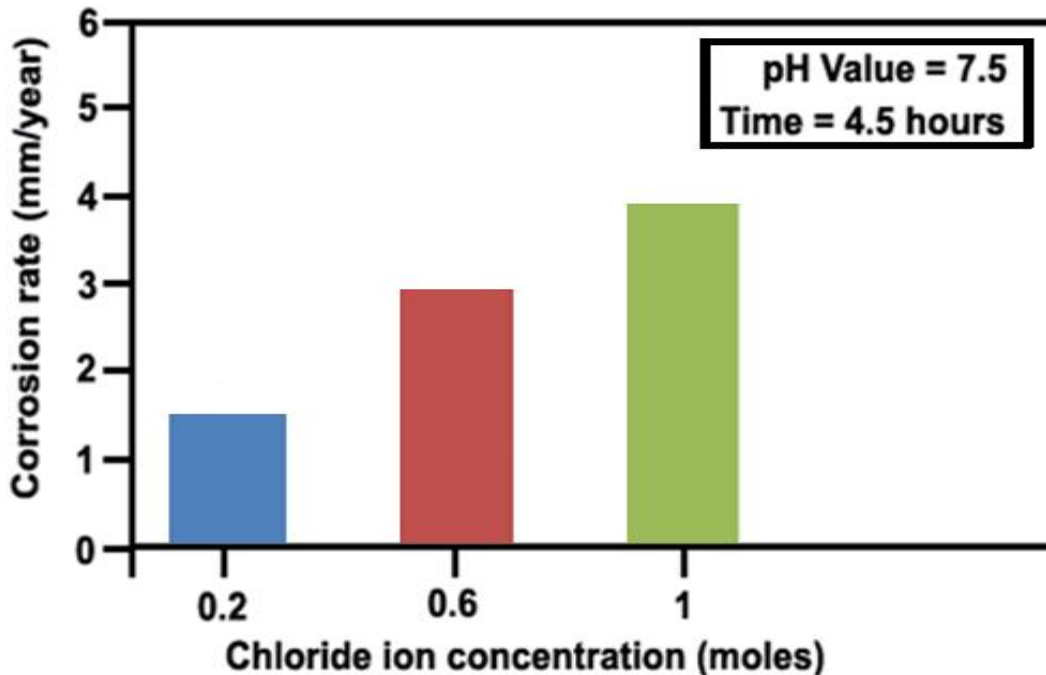


Fig.14 Effect of exposure time on corrosion rate

VI. CORROSION PRODUCTS CHARACTERISTICS

Fig. 18 shows the backscattered scanning electron micrographs of the transversal sections of the AZ31B magnesium alloys after 4.5 h of exposure in NaCl solution. A thick and loose corrosion layer, possibly consisting of $Mg(OH)_2$, was observed for the AZ31 alloy. Fig. 19 shows the low angle XRD study of test materials immersed in NaCl solution for 4.5 h. The main corrosion product was brucite, $Mg(OH)_2$ (JCPDS 86-0441). Peaks of hydrated magnesium carbonate hydroxide (hydromagnesite $Mg_5(CO_3)_4(OH)_2 \cdot 4H_2O$) were also detected for the AZ31B alloy, which possibly forms through the reaction of $Mg(OH)_2$ with atmospheric CO_2 (Schluter et al., 2010).

A typical SEM cross-sectional micrograph of the Al_2O_3 coated samples after potentiodynamic polarization assay is shown in Fig.20. The corrosion of the specimen was not severe and was found in particular coating areas. The EDS

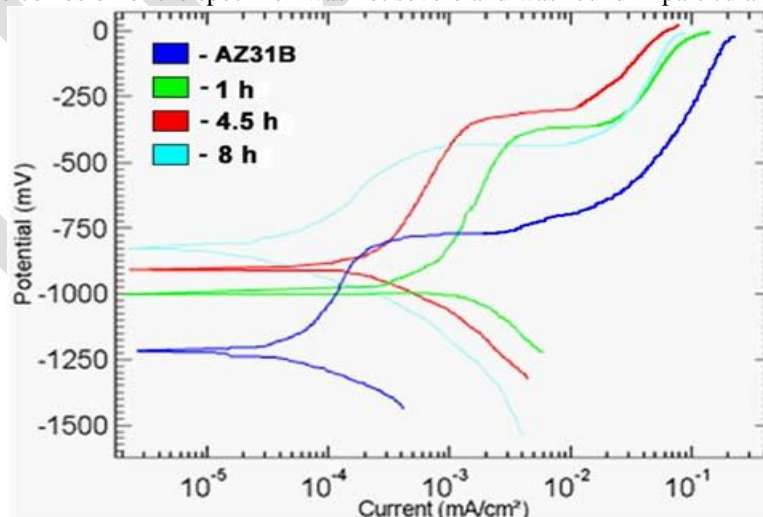


Fig.15 Effect of exposure time on tafel plot

International Journal of Innovative Research in Science, Engineering and Technology

(An ISO 3297: 2007 Certified Organization)

Vol. 3, Issue 12, December 2014

analysis traced about 1 at.% chlorine and 39 at.% oxygen in the dark regions. These regions in the coating were formed during the corrosion process in the standard three-electrode glass cell. To further illustrate the effects of barrier or pore resistance, the coated samples were analyzed after the accelerated exposure test. The results showed that after 4.5 h exposure, weight loss values became higher which confirms that the effect of barrier or pore resistance could be significantly improved during exposure. This improvement is attributed to the pore sealing by corrosion products during exposure which is in a good agreement with statements reported by Rodriguez et al. (2007).

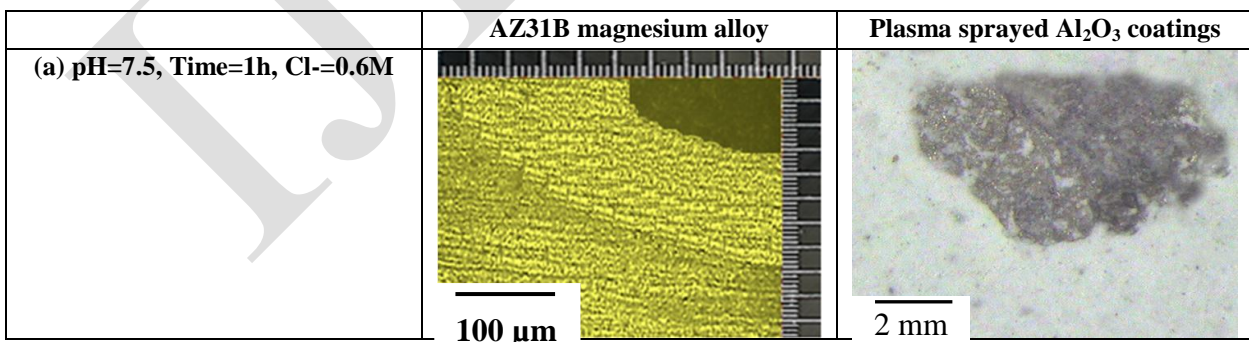
Fig.21 shows the XRD pattern of the coating after 4.5 h exposure. Identification of the peaks revealed that the phase composition of the surface of the coating is pure aluminum, aluminium oxide (AlO) and bayerite (Al(OH)₃) (JCPDS 33-0018).

According to the weight loss measurements of the coating, anti-corrosion performance of the coating can be improved by increasing the exposure time. This is due to the plugging of defects such as porosities, which are inherent characteristic of the thermally sprayed coatings. Plugging of defects occurs by the corrosion products which suppresses more penetration of the electrolyte into the coating. This could be the main reason for increasing the weight loss values during exposure (Verdian et al., 2010).

VII. CONCLUSIONS

The following important conclusions are obtained from this investigation

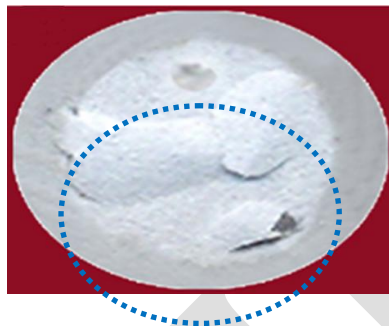
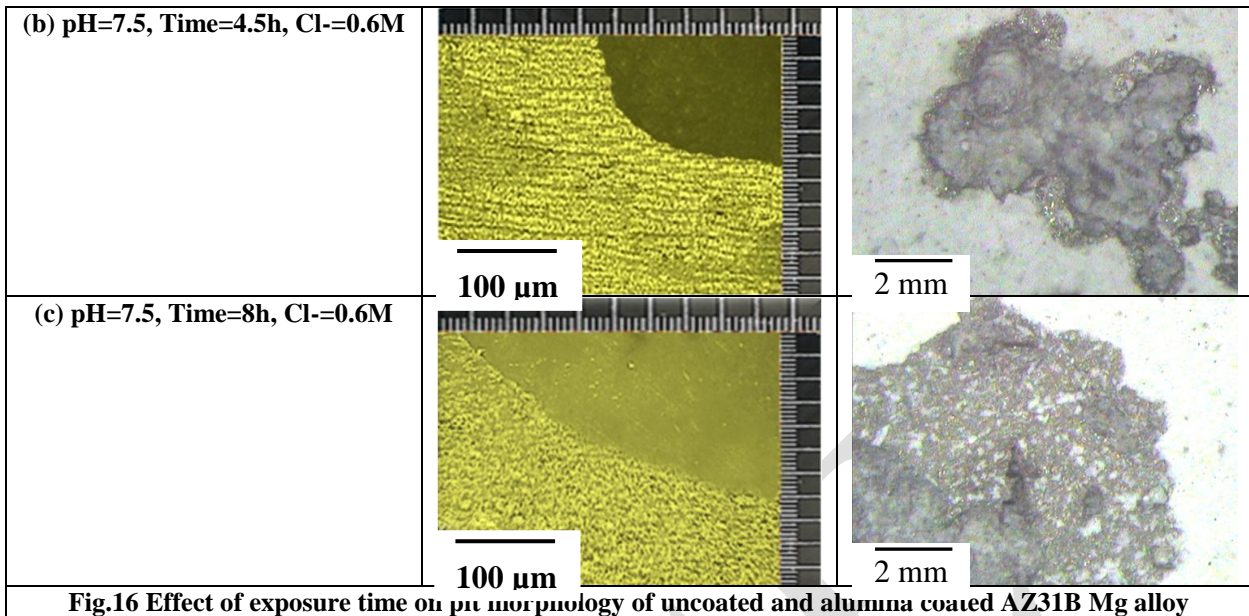
1. Empirical relationship was established to predict the corrosion rate of plasma sprayed alumina coatings on AZ31B magnesium alloy, incorporating chloride ion concentrations, pH value and exposure time. The developed relationship can be effectively used to predict the corrosion rate of alumina coatings on AZ31B magnesium alloy at 95% confidence level.
2. In acidic NaCl solution (pH 3), the Al₂O₃ coatings could not provide sufficient corrosion protection to magnesium alloy substrate in longer exposures. On the other hand, the more stable corrosion resistance of the coating than that in neutral solution was observed in alkaline NaCl solution.
3. Alumina coatings were found to be highly susceptible to localized damage, and could not provide an effective corrosion protection to Mg alloy substrate in solutions containing higher chloride concentrations. Furthermore, the corrosion potential shifted more negative (more negative) values with the increase of chloride ion concentration. The level of the corrosion attack of alumina coated AZ31 alloy is much higher when chloride ion concentration is greater than 0.6M, which was validated by the surface micrographs.
4. The corrosion resistance was formed in the alumina coated specimens with the increased exposure time period. A corrosion resistivity prevails with the increase of exposure time, resulting with the formation of passive film layer as a dominant factor to avoid the corrosion further.



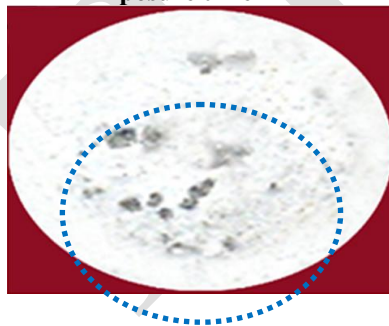
**International Journal of Innovative Research in Science,
Engineering and Technology**

(An ISO 3297: 2007 Certified Organization)

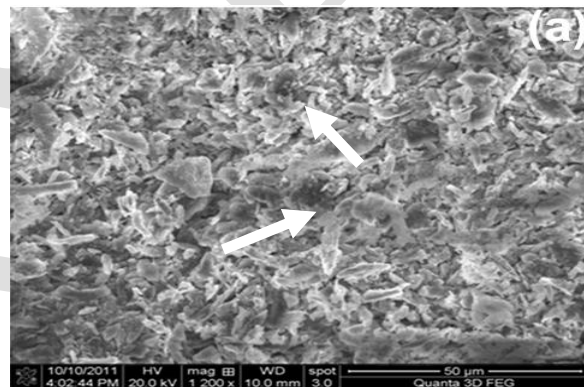
Vol. 3, Issue 12, December 2014



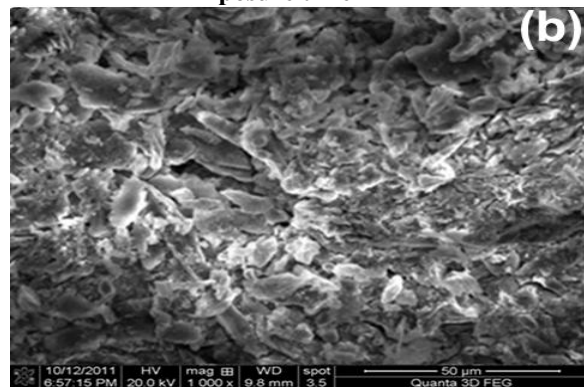
Exposure time = 1h



Exposure time = 4.5h



Exposure time = 1h

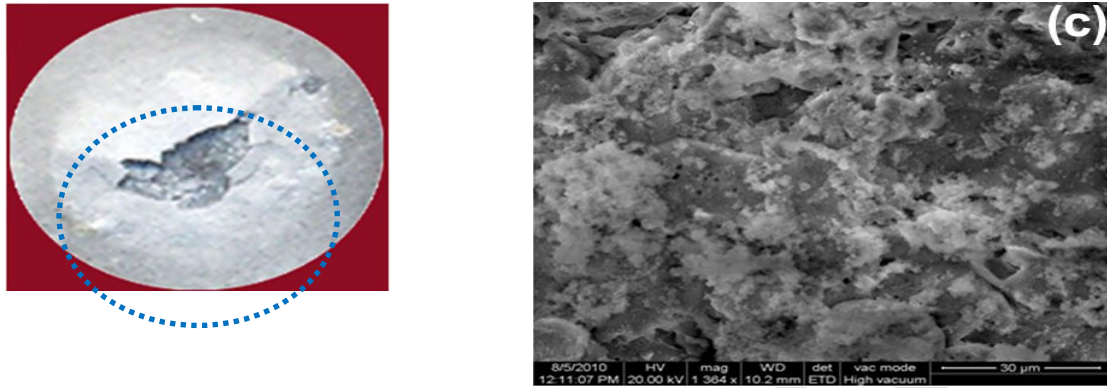


Exposure time = 4.5h

**International Journal of Innovative Research in Science,
Engineering and Technology**

(An ISO 3297: 2007 Certified Organization)

Vol. 3, Issue 12, December 2014



(a) Surface morphology
(Lower magnification)

(b) Optical micrographs
(Higher magnification)

Fig.17 Effect of exposure time on corrosion morphology of alumina coatings on AZ31B magnesium alloy

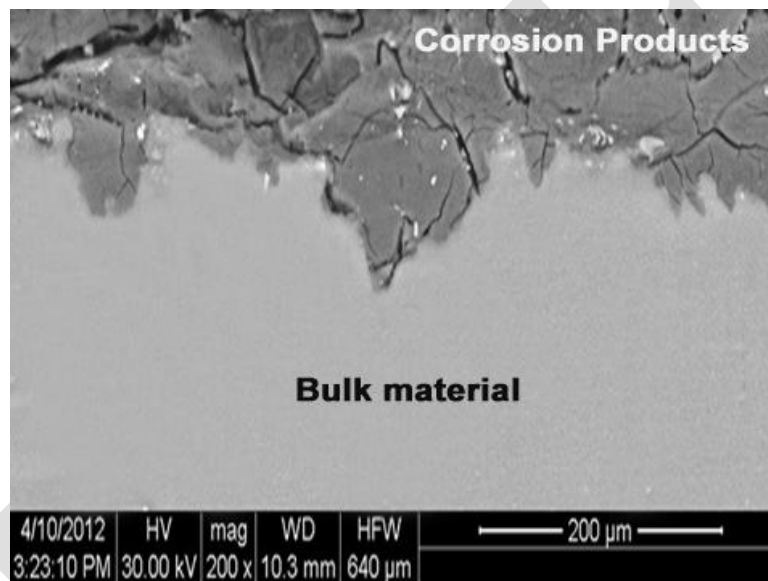


Fig. 18 BSE micrographs of the cross-sections of AZ31B magnesium alloy after immersion in NaCl for 4.5 h.

**International Journal of Innovative Research in Science,
Engineering and Technology**

(An ISO 3297: 2007 Certified Organization)

Vol. 3, Issue 12, December 2014

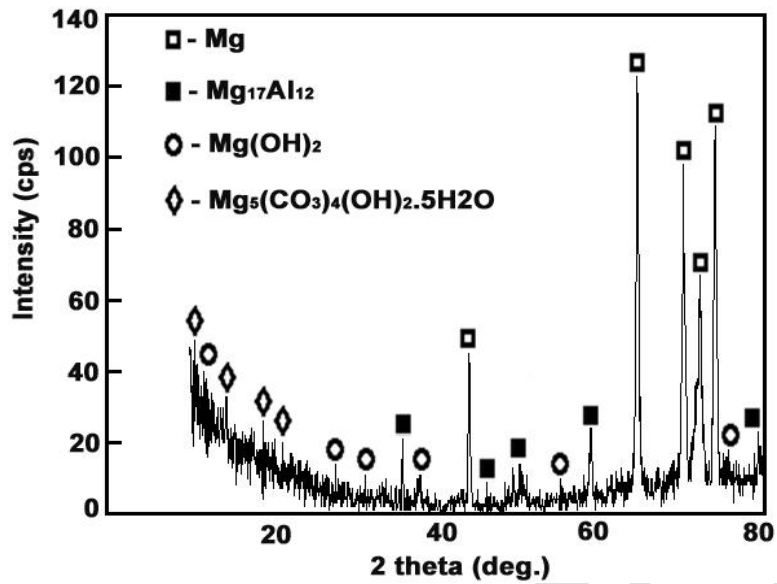


Fig. 19 XRD study of AZ31B specimens immersed in NaCl for 4.5 h

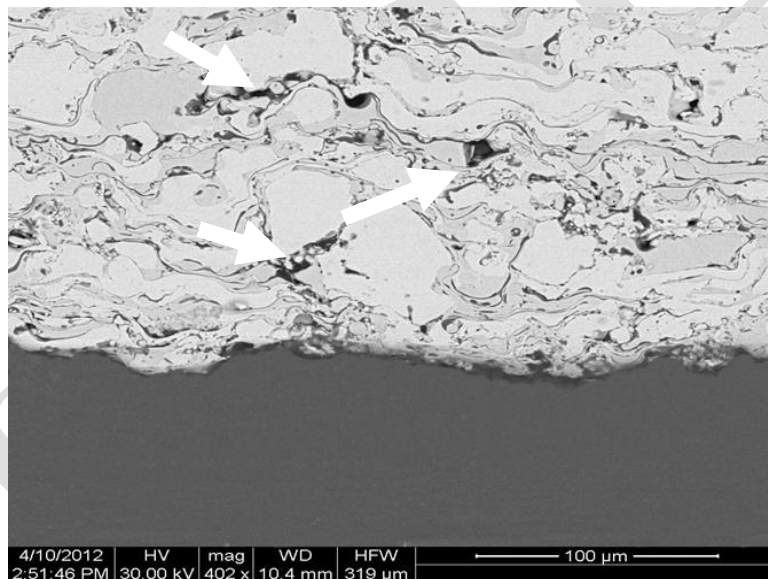


Fig. 20 The backscattered SEM micrograph of the cross section of alumina coating in sodium chloride solution for 4.5 h

International Journal of Innovative Research in Science, Engineering and Technology

(An ISO 3297: 2007 Certified Organization)

Vol. 3, Issue 12, December 2014

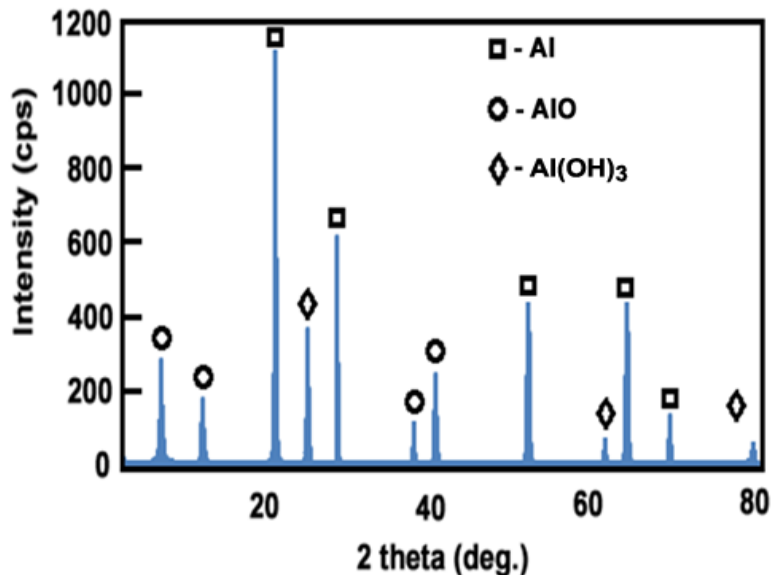


Fig. 21 XRD pattern of the alumina coating after 4.5 h immersion in NaCl solution

ACKNOWLEDGMENT

The authors are grateful to the Department of Manufacturing Engineering, Annamalai University, Annamalai Nagar, India, for extending the facilities of Material Testing Laboratory to carry out this investigation. Authors would like to thank Dr. C.S. Ramachandran, Post doctoral research scholar, State University of Newyork, USA and Mr. R. Selvendiran, Technical Assistant, Manufacturing Engineering for their help with deposition of the coatings.

REFERENCES

- [1] Ferrando, W. A., "Review of corrosion and corrosion control of magnesium alloys and composites", Journal of Materials Engineering, Vol. 11, pp. 299-313, 1989.
- [2] Song, G. L., Atrens, A., "Corrosion Mechanisms of Magnesium Alloys [Review]", Advanced Engineering Materials, Vol. 1, pp. 11-33, 1999.
- [3] Gray-Munro, J. E., Luan, B., and Huntington, L., "The influence of surface microchemistry in protective film formation on multi-phase magnesium alloys", Applied Surface Science, Vol. 254, pp.2871-2877, 2008.
- [4] Singh, H., Sidhu, B. S., Puri, D., and Prakash, S., "Use of plasma spray technology for deposition of high temperature oxidation/corrosion resistant coatings – a review", Materials and Corrosion, Vol. 58, pp. 92-102, 2007.
- [5] Gray, J. E., Luan, B., "Protective coatings on magnesium and its alloys — a critical review", Journal of Alloys and Compounds, Vol. 336, pp. 88-113, 2002.
- [6] Blawert, C., Dietzel, W., Ghali, E., and Song, G., "Anodizing Treatments for Magnesium Alloys and Their Effect on Corrosion Resistance in Various Environments", Advanced Engineering Materials, Vol. 8, pp. 511-533, 2006.
- [7] Singh, A., Harimkar, S. P., "Laser Surface Engineering of Magnesium Alloys: A Review", JOM, Vol. 64, pp. 716-733, 2012.
- [8] Aruna, S. T., Balaji, N., Jyothi Shedthi., and William Grips, V. K., "Effect of critical plasma spray parameters on the microstructure, microhardness and wear and corrosion resistance of plasma sprayed alumina coatings", Surface and Coatings Technology, Vol. 208, pp. 92-100, 2012.
- [9] Wang, Y., Jiang, S., Wang, M. D., Wang, S. H., Xiao, T. D., and Strutt, P. R., "Abrasive Wear Characteristics of Plasma Sprayed Nanostructured Alumina/Titania Coatings", Wear, Vol. 237, pp. 176-185, 2000.
- [10] Sarikaya, O., "Effect of the Substrate Temperature on Properties of Plasma Sprayed Al₂O₃Coatings", Materials and Design, vol. 26, pp. 53-57, 2005.
- [11] Zhe Liu., Yanchun Dong., Zhenhua Chu., Yong Yang., Yingzhen Li., and Dianran Yan., "Corrosion behavior of plasma sprayed ceramic and metallic coatings on carbon steel in simulated seawater", Materials and Design, vol. 52, pp. 630-637, 2013.
- [12] Sugehis Liscano., Linda Gila., and Mariana H. Staia., "Effect of sealing treatment on the corrosion resistance of thermal sprayed ceramic coatings", Surface and Coatings Technology, vol. 188, pp. 135-139, 2004.
- [13] Arrabal, R., Matykina, E., Hashimoto, T., Skeldon, P., and Thompson, G. E., "Characterization of AC PEO coatings on magnesium alloys", Surface and Coatings Technology, vol. 203, pp. 2207-2220, 2009.
- [14] Inoue, H., Sugahara, K., Yamamoto, A., and Tsubakino, H., "Corrosion rate of magnesium and its alloys in buffered chloride solution", Corrosion Science, Vol. 44, pp. 603-10, 2002.

International Journal of Innovative Research in Science, Engineering and Technology

(An ISO 3297: 2007 Certified Organization)

Vol. 3, Issue 12, December 2014

- [15] GUO Hui-xia., MA Ying., WANG Jing-song., WANG Yu-shun., DONG Hai-rong., and HAO Yuan., "Corrosion behavior of micro-arc oxidation coating on AZ91D magnesium alloy in NaCl solutions with different concentrations", Transactions of Nonferrous Metals Society of China, Vol.22, pp. 1786 -1793, 2012.
- [16] Martin, H., Horstemeyer, M. F., and Wang, P., "Comparison of corrosion pitting under immersion and salt-spray environments on an as-cast AE44 magnesium alloy", Corrosion Science, Vol.52, pp. 3624–3638, 2010.
- [17] Zhao, M. C., Liu, M., Song, G. L., and Atrens, A., "Influence of pH and chloride ion concentration on the corrosion of Mg alloy ZE41", Corrosion Science, Vol. 50, pp. 3168–3178, 2008.
- [18] Nandini Dinodi, A., and Nityananda Shetty., "Electrochemical investigations on the corrosion behaviour of magnesium alloy ZE41 in a combined medium of chloride and sulphate", Journal of Magnesium and alloys, Vol. 1, pp. 201–209, 2013.
- [19] Nobuyoshi Hara., Yasuhiro Kobayashi., Daisuke Kagaya., and Noboru Akao., "Formation and breakdown of surface films on magnesium and its alloys in aqueous solutions", Corrosion Science, Vol. 49, pp. 166–175, 2007.
- [20] Thirumalaikumarasamy, D., Shanmugam, K., Balasubramanian, V., "Influences of atmospheric plasma spraying parameters on the porosity level of alumina coating on AZ31B magnesium alloy using response surface methodology", Progress in Natural Science: Materials International, Vol. 22, pp. 468–479, 2012.
- [21] Thirumalaikumarasamy, D., Shanmugam, K., Balasubramanian, V "Developing an empirical relationship to predict corrosion rate of AZ31B magnesium alloy under sodium chloride environment", Transactions of the Indian Institute of Metals, Vol. 67, pp.19-32, 2014.
- [22] Khuri, A. I., and Cornell, J. A., "Response surfaces: design and analysis, New York, Marcel Dekker Ltd, 1996.
- [23] Miller, R. G., Freund, J. E., and Johnson, D. E., "Probability and statistics for engineers", New Delhi, Prentice Hall of India Pvt Ltd, 1999.
- [24] ASTM standard G 102, "Standard practice for calculation of corrosion rate and related information from electrochemical measurements", annual book of ASTM standards, ASTM international, 2004.
- [25] Kumar, S., Kumar, P., and Shan, H. S., "Effect of evaporative pattern casting process parameters on the surface roughness of Al-7% Si alloy castings", Journal of Materials Processing Technology, Vol. 182, pp. 615-623, 2007.
- [26] Benyounis, K. Y., and Olabi, A. G., "Optimization of different welding processes using statistical and numerical approaches —a reference guide", Advances in Engineering Software, Vol. 39, pp. 483–496, 2008.
- [27] Liang, J., Bala Srinivasan, P., Blawert, C., and Dietzel, W., "Influence of pH on the deterioration of plasma electrolytic oxidation coated AM50 magnesium alloy in NaCl solutions", Corrosion Science, Vol. 52, pp. 540–547, 2010.
- [28] Gou yin-ning., Huang wei-jiu., Zeng rong-chang., and Zhu yi., "Influence of pH values on electroless Ni-P-SiC plating on AZ91D magnesium alloy", Transactions of Nonferrous Metals Society of China, Vol. 20, pp. 674-678, 2010.
- [29] Yun TIAN., Li-jing YANG., Yan-fang LI., Ying-hui WEI., Li-feng HOU., Yong-gang LI., Ri-Ichi MURAKAMI., "Corrosion behaviour of die-cast AZ91D magnesium alloys in sodium sulphate solutions with different pH values", Transactions of Nonferrous Metals Society of China, Vol. 21, pp. 912-920, 2011.
- [30] Liang, J., Bala Srinivasan, P., Blawert, C., and Dietzel, W., "Influence of chloride ion concentration on the electrochemical corrosion behaviour of plasma electrolytic oxidation coated AM50 magnesium alloy", Electrochimica Acta, Vol. 55, pp. 6802–6811, 2010.
- [31] Yang Yue., and Wu Hua., Effect of current density on corrosion resistance of micro-arc oxide coatings on magnesium alloy, Transactions of Nonferrous Metals Society of China, Vol. 20, pp. 688-692, 2010.
- [32] Song, S., Shen, W. D., Liu, M. H., and Song, G. L., "Corrosion study of new surface treatment/coating for AZ31B magnesium alloy", Surface Engineering, Vol. 28, pp. 486-490, 2012.
- [33] Suegama, P. H., Fugivara, C. S., Benedetti, A. V., Fernandez, J., Delgado, J., and Guilemany, J. M., "Electrochemical behavior of thermally sprayed stainless steel coatings in 3.4% NaCl", Corrosion Science, Vol. 47, pp. 605-620, 2005.
- [34] You Wang., Wei Tian., Tao Zhang., and Yong Yang., "Microstructure, spallation and corrosion of plasma sprayed Al₂O₃-13%TiO₂ coatings", Corrosion Science, Vol. 51, pp. 2924-2931, 2009.
- [35] Schluter, K., Zamponi, C., Piorra, A., and Quandt, E., "Comparison of the corrosion behaviour of bulk and thin film magnesium alloys," Corrosion Science, Vol. 52, pp. 3973–3977, 2010.
- [36] Rodriguez, R. M., Paredes, R. S. C., Wido, S. H., and Calixto, A., "Comparison of aluminum coatings deposited by flame spray and by electric arc spray", Surface and Coatings Technology, Vol. 202, pp. 172-179, 2007.
- [37] Verdian, M. M., Raeissi, K., and Salehi, M., "Corrosion performance of HVOF and APS thermally sprayed NiTi intermetallic coatings in 3.5% NaCl solution", Corrosion Science, Vol. 52, pp. 1052-1059, 2010.